
HADL FRAMEWORK FOR NOISE RESILIENT LONG-TERM TIME SERIES FORECASTING

Aditya Dey

Department of Data Science
Norwegian University of Life Sciences (NMBU)
Aas, Norway 1432
aditya.dey@nmbu.no

Jonas Kusch

Department of Data Science
Norwegian University of Life Sciences (NMBU)
Aas, Norway 1432
jonas.kusch@nmbu.no

Fadi Al Machot

Department of Data Science
Norwegian University of Life Sciences (NMBU)
Aas, Norway 1432
fadi.al.machot@nmbu.no

February 18, 2025

ABSTRACT

Long-term time series forecasting is critical in domains such as finance, economics, and energy, where accurate and reliable predictions over extended horizons drive strategic decision-making. Despite the progress in machine learning-based models, the impact of temporal noise in extended lookback windows remains underexplored, often degrading model performance and computational efficiency. In this paper, we propose a novel framework that addresses these challenges by integrating the Discrete Wavelet Transform (DWT) and Discrete Cosine Transform (DCT) to perform noise reduction and extract robust long-term features. These transformations enable the separation of meaningful temporal patterns from noise in both the time and frequency domains. To complement this, we introduce a lightweight low-rank linear prediction layer that not only reduces the influence of residual noise but also improves memory efficiency. Our approach demonstrates competitive robustness to noisy input, significantly reduces computational complexity, and achieves competitive or state-of-the-art forecasting performance across diverse benchmark datasets. Extensive experiments reveal that the proposed framework is particularly effective in scenarios with high noise levels or irregular patterns, making it well suited for real-world forecasting tasks. The code is available in <https://github.com/forged-master/HADL>.

1 Introduction

Real-world time series data from domains such as finance [1], economics [2], and energy systems [3] rely on accurate long-term forecasting to support informed decision-making that has a significant impact on global development [4]. However, these datasets often contain significant levels of temporal noise due to their highly volatile nature [5], environmental factors [6], and random fluctuations. This poses a critical challenge for Long-term Time Series Forecasting (LTSF) models, as they can obscure the underlying patterns and reduce the accuracy of the predictions [7]. Thus, a systematic study of temporal noise in LTSF and its effects on model accuracy is required.

Most LTSF transformer models can perform well with a small lookback window due to the large parameter size and the benefits of using vanilla or modified attention [8, 9, 10]. However, the gains in accuracy from increasing lookback windows are not significant [8], which may be due to temporal noise that obscures the underlying trend and seasonality patterns. This highlights the trade-off between a large lookback window, parameter size, and temporal noise, where increasing the lookback window or parameter size may not yield significant accuracy gains due to noise.

Although these large-parameter models perform well with a small lookback window, low-parameter Multi-layer Perceptron (MLP) models with a larger lookback window have matched or outperformed them while using fewer parameters and lower computational complexity [11, 12]. An analysis of these models suggests that underlying temporal patterns in time series can be extracted using simple attention [13], trend-seasonality decomposition [7, 12], or time-to-frequency domain conversions [11]. The success of these low-parameter models challenges the conventional reliance on large parameters, demonstrating that accurate LTSF is achievable with streamlined architectures.

These low-parameter models, though computationally efficient, also face a trade-off between lookback window size and temporal noise. A small lookback window may not provide sufficient information, and a larger window is susceptible to temporal noise [7]. Hence, these models are based on a sufficiently large lookback to achieve good performance [11, 12].

Thus, to address the challenges of noise robustness, lightweight design, and accuracy improvement in LTSF, we propose the HADL framework. This framework employs Discrete Wavelet Transform (DWT) with a Haar wavelet to reduce the effects of noise in a large lookback window, effectively compressing the input length by half through approximation coefficients. The compressed series is then transformed into the frequency domain using Discrete Cosine Transform (DCT), enabling high-resolution extraction of underlying patterns. Finally, a low-rank layer improves generalization while maintaining minimal memory requirements. We avoid channel mixing, which can accidentally project the noise from one series onto another [8] and utilize a general layer instead of a per channel layer, which helps to reduce the risk of overfitting by sharing parameters across channels.

The HADL framework integrates DWT, DCT, and a low-rank layer, offering the following advantages:

- DWT reduces noise and compresses the input, enabling a lightweight model with fewer parameters.
- DCT enhances the extraction of long-term temporal patterns while reducing computational overhead.
- Low-rank layers improve generalization and noise robustness while further minimizing parameter requirements.
- A single prediction layer reduces overall complexity, ensuring that the model remains lightweight and interpretable.

This framework achieves accuracy comparable to or better than other State of the Art (SOTA) models while significantly reducing parameter size and effectively mitigating noise. The result is a lightweight, robust model specifically designed to perform well on real-world noisy datasets with highest accuracy.

2 Related Works

2.1 MLP-Based Models for Lightweight Forecasting

MLP models offer computationally efficient and interpretable alternatives, often achieving predictive performance that is comparable to or superior to other approaches [7, 11, 13]. For example, DLinear [7] applies trend and seasonality decomposition, whereas FITS [11] achieves higher accuracy using Discrete Fourier Transform (DFT) with approximately 5K parameters. Similarly, SparseTSF [12], an ultra-lightweight model with approximately 1K parameters, effectively utilizes cross-period sparse techniques to extract periodic features. Other notable MLP-based models, such as TSMixer [13], LightCTS [14], and FreTS [15], may not be as lightweight as SparseTSF but nevertheless deliver competitive performance.

Some of these models rely on techniques that extract periodicity in the time domain by selecting the period length as a hyperparameter [12, 15] or by converting the data into the frequency domain using the DFT [11, 15]. Time domain approaches often lack robust methods for reducing temporal noise, and the assumption that all features share the same periodicity set as a hyperparameter can lead to inaccuracies [12]. On the other hand, frequency-domain methods using DFT with cutoff frequencies to reduce temporal noise assume a uniform cutoff range for all features, which may impact accuracy.

2.2 Convolutional and Recurrent Neural Network Methods

Other classes of models, such as ModernTCN [16], employ dilated temporal convolutions to extract and enhance temporal characteristics, reaffirming the competitiveness of Convolutional Neural Network (CNN)s. Although not as lightweight as MLP models, ModernTCN demonstrates comparable runtime efficiency. Similarly, Recurrent Neural Network (RNN)-based models, such as SegRNN [17], xLSTM [18], and WiTRAN [19], excel in capturing temporal dependencies and sequence relationships. However, like other approaches, these models rely on appropriate lookback window sizes and large parameter counts, which may be affected by temporal noise.

2.3 Transformer-based Models

Most emerging LTSF models are transformer-based [20], with notable examples such as PatchTST, which demonstrates that modifications to the attention mechanism can be avoided by segmenting univariate time series into patches [8]. The iTransformer extends this concept further by treating each feature as a patch, allowing a receptive field that spans the entire length of the feature [9]. Although these patching techniques can enhance model performance, they also introduce challenges. For example, a noisy patch can obscure the underlying patterns. Similarly, in iTransformer, noisy features may impede the model’s ability to discern meaningful structures. These limitations underscore the sensitivity of patch-based methods to temporal noise, posing challenges to consistent performance.

Despite these challenges, transformer-based models continue to inspire advancement, with recent models, such as FredFormer [21] and FrNet [10], aiming to further enhance prediction accuracy. However, these transformers often require significant memory and computational resources, making them less practical for scenarios where efficiency is critical.

Low-rank implementations have not been widely studied in LTSF models. However, they have shown potential in vanilla transformers by improving generalization [22, 23, 24]. They have also been shown to enhance inter-channel dependencies in LTSF [25]. Incorporating low-rank techniques can improve performance in time series forecasting by efficiently capturing critical temporal patterns while reducing parameter complexity.

Currently, no LTSF models have simultaneously addressed noise robustness, accuracy improvement, and lightweight design in a unified manner.

3 The Proposed Method

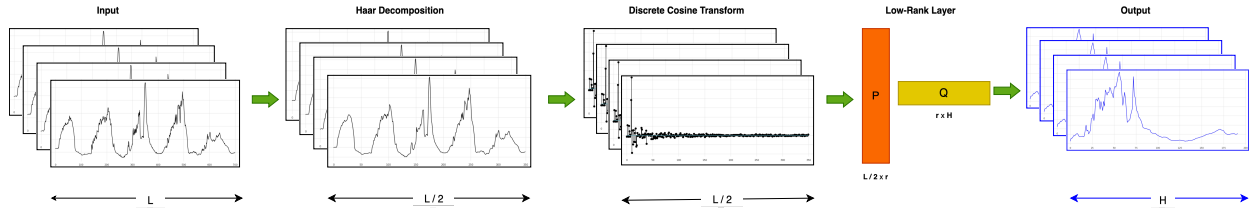


Figure 1: Illustration of the HADL architecture.

In this section, we provide a concise overview of the HADL framework, followed by a detailed explanation and rationale for the design choices.

Problem Definition: Given a regularly sampled multivariate time series with a lookback window L , represented as $X_T = x_1, \dots, x_t, \dots, x_L \in \mathbb{R}^{C \times L}$, where each time step x_t is a vector of dimension C , the objective is to forecast future values $\hat{Y}_T = x_{L+1}, \dots, x_{L+\tau}, \dots, x_{L+H} \in \mathbb{R}^{C \times H}$ over a horizon of length H .

Summary: The multivariate time series $X_T \in \mathbb{R}^{C \times L}$ is first transformed by DWT using Haar wavelet to obtain approximation coefficient values $A_T \in \mathbb{R}^{C \times \frac{L}{2}}$, effectively compressing the input length by half while removing the detail coefficient values to mitigate the impact of noise. Next, the time domain representation A_T is converted into the frequency domain $A_F \in \mathbb{R}^{C \times \frac{L}{2}}$ using the DCT, allowing the model to extract long-term periodic features at high-frequency resolution. Finally, the frequency representation A_F is processed through a low-rank layer to predict the target $\hat{Y} \in \mathbb{R}^{C \times H}$ in the time domain, eliminating the need for an explicit inverse transform.

$$A_{T,-} = \text{DWT}(X_T) \quad (1a)$$

$$A_F = \frac{2}{L} \times \text{DCT}(A_T) \quad (1b)$$

$$\hat{Y}_T = \text{LowRankLayer}(A_F) \quad (1c)$$

The complete architecture of the HADL framework is illustrated in Figure 1. The transformation and prediction processes are formally described by the equations in (1) and the algorithm presented in Appendix B.

3.1 Discrete Wavelet Transform

The trend-seasonality decomposition in the time domain provides high temporal resolution but relies heavily on accurately selecting the seasonal window to capture periodic patterns [7, 12]. An incorrect choice of window size can lead to temporal leakage or distortion of periodic components. In contrast, the DFT offers high-frequency resolution [11, 15] but operates under the implicit assumption that the observed time series represents a complete cycle of a single period [26]. Violating this assumption results in spectral leakage, which distorts the frequency components. A balanced resolution in both the time and frequency domains can be achieved through methods like Short Time Fourier Transform (STFT) or DWT, which provide multiresolution decomposition at the cost of increased dimensionality.

The key advantage of DWT over STFT lies in the orthogonality of wavelet functions, which ensures that at each level of decomposition, distinct frequency components are captured [27]. This property eliminates redundancy and improves the interpretability of transformed data, addressing the main limitation of STFT, where overlapping windowed components can redundantly capture the same frequency across multiple levels.

Therefore, our method begins with DWT to decompose the time series. Among various wavelet families, we choose the Haar wavelet because of its simplicity and interpretability. The Haar wavelet performs convolution on the time series with two sets of filters: an approximation filter and a detail filter with a kernel size of 2 and a stride of 2. The approximation filter is an averaging operator, while the detail filter acts as a differencing operator. For our purposes, we use the approximation coefficients $A_T \in \mathbb{R}^{C \times \frac{L}{2}}$, which capture essential information while reducing noise. The detail coefficients $D_T \in \mathbb{R}^{C \times \frac{L}{2}}$, which mainly represent noise, are discarded.

$$A_T = X_T * \left[\frac{1}{\sqrt{2}}, \frac{1}{\sqrt{2}} \right] \quad (2)$$

$$D_T = X_T * \left[-\frac{1}{\sqrt{2}}, \frac{1}{\sqrt{2}} \right] \quad (3)$$

Although it is possible to use detail coefficients for prediction with linear layers, doing so would increase the model’s complexity and parameter count without substantial benefits.

We limit the decomposition to a single level to avoid excessive smoothing, which can eliminate critical frequency components necessary for accurate forecasting. For lookback windows in the typical range of 336 to 720, a single level of decomposition is sufficient. However, multiple decomposition levels may be considered for ultra-long lookback windows. Additionally, employing linear layers across multiple decomposition levels significantly increases computational complexity and may not provide substantial improvements in feature extraction.

3.2 Discrete Cosine Transform

DFT and DCT share a common mathematical foundation but differ in their focus and application. DFT represents a signal using both real and imaginary components. The cosine component captures smooth, low-frequency variations, while the sine component highlights abrupt changes and high-frequency components [26]. Although this dual representation is comprehensive, the DCT’s exclusive focus on cosine components leads to energy compaction, in which most of the signal’s energy is concentrated in fewer coefficients [28, 29]. This makes DCT particularly effective in representing long-term patterns in LTSF while avoiding the additional complexity introduced by imaginary parts.

Thus, the approximation coefficients $A_T \in \mathbb{R}^{C \times \frac{L}{2}}$ undergo DCT Type II conversion, generating an output $A_F \in \mathbb{R}^{C \times \frac{L}{2}}$ with high-frequency resolution. This transformation is accompanied by length-based normalization ($\frac{1}{L}$), ensuring that the resulting frequency domain representation is scale-independent and numerically stable.

$$A_F = \frac{2}{L} \cdot \text{DCT}(A_T) \quad (4)$$

When DCT is applied after DWT instead of directly on the original time series, the process offers distinct advantages. The approximation coefficients from DWT provide a smoothed, noise-reduced representation of the data. This preprocessing ensures that the DCT operates on a cleaner input, avoiding distortions caused by high-frequency noise in the original series. Additionally, reducing the series length decreases the computational complexity of the DCT operation and focuses the analysis on the most informative components of the signal, ensuring that critical long-term periodic features are emphasized.

This combination is advantageous in real-world forecasting as it balances noise robustness, computational efficiency, and the extraction of long-term dependencies and periodic structures.

3.3 Low Rank Layer

Most models in LTSF employ standard linear layers for the final prediction; however, using a low-rank layer offers several advantages. Low-rank layers have a significantly reduced memory footprint during training and inference. Moreover, a reduced memory footprint directly leads to fewer operations required to train and evaluate the network.

There are different approaches to defining a low-rank layer. Perhaps the most common strategy for defining a low-rank layer is selecting two matrices: $P \in \mathbb{R}^{\frac{L}{2} \times r}$ and $Q \in \mathbb{R}^{r \times H}$, where r represents the rank of the layer ($r \ll \min(\frac{L}{2}, H)$) [22]. These matrices jointly form a low-rank approximation of the weight matrix $W \approx PQ$, which significantly reduces the number of trainable parameters. In addition, a bias vector $B \in \mathbb{R}^H$ is included to account for linear shifts. The low-rank layer then takes the form:

$$\hat{Y}_T = A_F P Q + B. \quad (5)$$

Standard gradient-based optimization methods are used to train P , Q , and B . The corresponding gradient flow for a loss function $\mathcal{L}(PQ)$ (where we omit dependence on the bias and A_F for ease of presentation) then reads

$$\dot{P}(t) = -\nabla_P \mathcal{L}(P(t)Q(t)), \quad (6a)$$

$$\dot{Q}(t) = -\nabla_Q \mathcal{L}(P(t)Q(t)). \quad (6b)$$

Here, $\nabla_{P,Q}$ denotes the gradients with respect to the respective low-rank factors. If the method converges to a stationary point of (6) at time t_* and $W(t_*) := P(t_*)Q(t_*)$ satisfies the gradient flow equation $\dot{W} = -\nabla_W \mathcal{L}(W)$ at time t_* , then $\nabla_W \mathcal{L}(W(t_*)) = 0$ since

$$\begin{aligned} \nabla_W \mathcal{L}(W(t_*)) &= -\dot{W}(t_*) \\ &= -\dot{P}(t_*)Q(t_*) - P(t_*)\dot{Q}(t_*) = 0. \end{aligned}$$

In this case, the stationary point fulfills the necessary condition of a local full-rank optimum. A primary advantage of low-rank layers is their computational efficiency, which results from the fewer operations required to compute (5). This lower computational cost in the forward pass directly translates into fewer evaluations in the backward pass, leading to shorter training time. In addition to computational efficiency, low-rank networks have been observed to outperform their dense counterparts [30, 31]. This observation is not yet rigorously understood, but it is assumed that the regularization imposed by low-rank compression improves the generalization of the resulting networks. In Section 6.2, we study the regularization effects of low-rank networks and show that similar behavior can be observed in our experiments.

3.4 Key Features

A distinctive feature of our framework is the omission of the inverse transformation from the frequency domain to the time domain. This simplification is justified by Parseval’s theorem, as shown in Equation (7), which ensures energy conservation between the time and frequency domains [15].

$$\sum_{n=0}^{N-1} |(A_T)_n|^2 = \frac{1}{N} \sum_{n=0}^{N-1} |(A_F)_n|^2 \quad (7)$$

As a result, the model operates directly in the frequency domain, capturing necessary relationships without the added complexity of domain conversion. This design choice enhances computational efficiency and interpretability while preserving the fidelity of the original time series.

Additionally, the framework employs a single generalized low-rank layer instead of separate layers for each feature or channel. This design reduces parameter redundancy, mitigates overfitting to specific channels, and enhances overall model efficiency. With the low-rank layer as the only trainable component, the model achieves a compact architecture that balances simplicity with effective noise mitigation. This streamlined approach makes the HADL framework particularly suitable for LTSF tasks, offering both accuracy and computational efficiency.

To further mitigate overfitting and reduce noise influence, L1 regularization is incorporated. This regularization shrinks the coefficients of less important features, contributing to a more robust and generalizable model.

4 Experiments

We conduct a standard LTSF test for prediction lengths $H = \{96, 192, 336, 720\}$, using a fixed lookback window of $L = 512$ for all baseline models.

Additionally, we conduct a robustness test by introducing noise into the training data ($X_{\text{train}}, y_{\text{train}}$) as follows:

$$X_{\text{train}} := X_{\text{train}} + \mathcal{N}(0, 1) \cdot \eta \quad (8)$$

Here, $\mathcal{N}(0, 1)$ represents random noise sampled from a standard normal distribution, and $\eta = \{0.0, 0.3, 0.7, 1.7, 2.3\}$ controls the noise intensity. The validation and test datasets remain unchanged to ensure consistent evaluation of the model’s robustness.

Settings All experiments were conducted using the PyTorch [32] and SciPy [33] frameworks on an NVIDIA Quadro RTX 8000 GPU with 100 GB of memory. The models were trained using the ADAM optimizer for 100 epochs with a patience of 20 epochs for multivariate forecasting and 50 epochs with a patience of 10 epochs for robustness testing.

Datasets We evaluate our model on four widely used benchmark datasets: ETT [34] (ETTh1, ETTh2, ETTm1, ETTm2) and Traffic [35]. Detailed descriptions of these datasets are provided in Appendix A.

Baseline Models We compare our approach against several recent and highly successful SOTA models, including PatchTST [8], iTransformer [9], FrNet [10], DLinear [7], SparseTSF [12], FreTS [15], and ModernTCN [16].

Evaluation Metrics Prediction errors for multivariate forecasting and robustness testing are evaluated using Mean Squared Error (MSE) and Mean Absolute Error (MAE).

For multivariate forecasting, we report Improvement (Imp.), which quantifies the error reduction achieved by our model compared to the best-performing baseline model. This is calculated as the difference between the MSE of the best baseline model ($\text{MSE}_{\text{baseline}}$) and the MSE of our model (MSE_{ours}). A higher positive improvement value indicates that our model performs significantly better than the baseline, while a lower or negative value suggests comparable or worse performance.

$$\text{Imp.} = \text{MSE}_{\text{baseline}} - \text{MSE}_{\text{ours}} \quad (9)$$

For robustness testing, we introduce the concept of Noise-Resilience Relative (NRR) to better evaluate the impact of increasing noise intensity. NRR quantifies the deviation in prediction error as the noise intensity increases, offering a clear perspective on the model’s robustness.

$$\text{NRR} = \frac{\text{MSE}_{\eta=x}}{\text{MSE}_{\eta=0.0}} \quad (10)$$

$$\text{MAV} = \frac{1}{n} \sum_{i=1}^n |\text{NRR}_i - 1| \quad (11)$$

This metric allows us to compare the model’s performance under noisy conditions ($\eta = x$) with its baseline performance ($\eta = 0.0$). To summarize the overall performance of the model across varying noise intensities, we compute the Mean Absolute Variability (MAV) of the NRR with central point of 1. A lower MAV indicates that the model maintains consistent performance as the noise increases, demonstrating robustness.

5 Results

In this section, we discuss Multivariate Forecasting and Robustness Testing, followed by a combined analysis.

Multivariate Forecasting Table 1 highlights HADL’s strengths in long-term multivariate forecasting in various datasets. It achieves competitive or superior performance compared to baseline models while maintaining significantly fewer trainable parameters and lower memory consumption (Table 2). The complete benchmark results, evaluated using MSE and MAE, are provided in Appendix D.1.

HADL ranks among the best performers, often achieving the best or second-best MSE. In ETTh2, it improves MSE by +0.001 to +0.003 across all horizons while using only 17–50K parameters, far fewer than FrNet (116–7486K). Across ETTh1, ETTh2 and ETTm1, it achieves mixed results (−0.001 to +0.012), maintaining efficiency over DLinear (1034–7756K) and PatchTST (706–5184K). Its lightweight design results in lower FLOPs (0.004–0.011B).

In the Traffic dataset, HADL struggles in high-dimensional settings, showing negative improvements (−0.045 to −0.048), where transformer-based models excel. However, its performance against DLinear remains close (0.002–0.006), indicating the effectiveness of its generalization approach in MLP based models. Notably, HADL outperforms SparseTSF, which, despite having the smallest parameter count (0.2–1.4K), fails to leverage minimal parameters effectively.

Robustness Testing Table 3 presents robustness testing results for HADL, across different noise intensities compared to baseline models. The full results are in Appendix D.3.

Table 1: Results for MSE (lower is better) in long-term time series forecasting on benchmark datasets. We compare HADL framework with (w) and without (w/o) regularization against baseline models using standard prediction lengths $H = \{96, 192, 336, 720\}$ and a lookback window $L = 512$ for all models. The best results are in **bold**, and the second best are underlined. "Imp." denotes the improvement compared to best-performing baseline model.

Model Type	Datasets H	ETTh1				ETTh2				ETTm1				ETTm2				Traffic			
		96	192	336	720	96	192	336	720	96	192	336	720	96	192	336	720	96	192	336	720
Transformer	PatchTST (2022)	0.394	0.424	0.457	0.461	0.292	0.347	0.380	0.431	<u>0.293</u>	<u>0.335</u>	0.368	0.423	<u>0.164</u>	0.223	0.277	0.381	0.489	0.498	0.506	0.541
	iTransformer (2023)	0.399	0.428	0.472	0.685	0.301	0.381	0.395	0.467	0.315	0.350	0.394	0.449	0.188	0.250	0.326	0.391	0.433	0.462	0.443	0.489
	FrNet (2024)	0.362	0.390	0.427	0.468	0.269	0.330	0.358	<u>0.391</u>	0.295	0.337	0.363	<u>0.421</u>	0.165	<u>0.221</u>	<u>0.274</u>	<u>0.360</u>	0.367	0.390	0.397	0.433
CNN	ModernTCN (2024)	0.472	0.498	0.507	0.531	0.300	0.348	0.384	0.410	0.313	0.363	0.392	0.447	0.169	0.232	0.307	0.385	<u>0.392</u>	<u>0.406</u>	<u>0.415</u>	<u>0.464</u>
MLP	DLinear (2023)	0.385	0.422	0.457	0.496	0.390	0.512	0.697	1.060	0.292	0.333	0.368	0.428	0.204	0.333	0.342	0.570	0.418	0.430	0.440	0.479
	SparseTSF (2024)	0.396	0.412	<u>0.426</u>	0.427	0.285	0.345	0.364	0.384	0.330	0.347	0.374	0.424	0.173	0.225	0.277	0.362	0.427	0.441	0.454	0.487
	FreTS (2024)	0.396	0.435	0.471	0.565	0.318	0.432	0.479	0.809	0.317	0.356	0.385	0.440	0.179	0.254	0.314	0.389	0.398	0.414	0.428	0.471
	HADL (w/o)	0.365	0.397	0.423	0.446	0.272	0.334	0.358	0.395	0.306	0.339	0.367	0.420	0.163	0.218	0.271	0.359	0.413	0.433	0.444	0.481
	HADL (w)	<u>0.363</u>	<u>0.395</u>	0.421	<u>0.444</u>	<u>0.271</u>	<u>0.334</u>	0.358	0.395	0.304	0.337	<u>0.365</u>	0.418	0.163	0.218	0.271	0.359	0.412	0.433	0.445	0.481
	Imp.	-0.001	-0.005	+0.005	-0.017	-0.002	-0.004	0.000	-0.011	-0.012	-0.005	-0.002	+0.003	+0.001	+0.003	+0.003	+0.001	-0.045	-0.043	-0.048	-0.048

Table 2: Results comparing FLOPs and total trainable parameters between HADL framework against baseline models on the ETTh1 and Traffic datasets for multivariate forecasting, using standard prediction lengths $H = \{96, 192, 336, 720\}$ and a lookback window $L = 512$ for all models.

Model Type	Dataset H	FLOPs ($\times 10^9$)								Parameters ($\times 10^3$)							
		ETTh1				Traffic				ETTh1				Traffic			
		96	192	336	720	96	192	336	720	96	192	336	720	96	192	336	720
Transformers	PatchTST (2022)	0.336	0.358	0.391	0.479	41.465	44.176	48.244	59.090	706.2	1395.0	2428.2	5183.4	84838.2	169659.0	296890.2	636173.4
	iTransformer (2023)	0.337	0.346	1.272	1.341	50.864	51.545	148.701	154.149	948.0	972.7	3592.0	3789.0	948.0	972.7	3592.0	3789.0
	FrNet (2024)	0.324	0.252	0.538	5.659	1.285	1.293	1.308	1.351	116.5	196.9	577.6	7485.9	81950.8	82614.8	83714.3	87254.8
CNN	ModernTCN (2024)	0.568	0.745	1.009	1.713	456.455	478.148	510.687	597.459	930.1	1716.7	2896.5	6042.6	10639.7	107326.3	108506.1	111652.2
MLP	DLinear (2023)	0.022	0.044	0.077	0.165	2.711	5.423	9.490	20.3337	1034.2	2068.4	3619.7	7756.5	127355.3	254710.6	445743.6	955164.9
	SparseTSF (2024)	0.002	0.003	0.004	0.007	0.324	0.409	0.536	0.875	0.2	0.4	0.6	1.4	0.2	0.4	0.6	1.4
	FreTS (2024)	3.778	3.783	3.792	3.814	14.539	14.561	14.592	14.677	16868.3	16892.9	16930.0	17028.6	16868.3	16892.9	16930.0	17028.6
	HADL	0.004	0.005	0.006	0.011	0.499	0.632	0.830	1.360	17.6	22.5	29.9	49.5	17.6	22.5	29.9	49.5

Table 3: Noise-Resilience Relative (NRR) and Mean Absolute (MAV) results for robustness testing on benchmark datasets, comparing HADL framework with (w) and without (w/o) regularization against baseline models. The tests are conducted using a lookback window of $L = 512$ and a prediction length of $H = 192$ under varying noise intensities $\eta = \{0.0, 0.3, 0.7, 1.3, 1.7, 2.3\}$. The best results are in **bold**, and the second best are underlined.

Model Type	η	ETTh1					ETTh2					ETTm1					ETTm2					Traffic				
		0.3	0.7	1.3	1.7	MAV	0.3	0.7	1.3	1.7	MAV	0.3	0.7	1.3	1.7	MAV	0.3	0.7	1.3	1.7	MAV	0.3	0.7	1.3	1.7	MAV
		NRR	NRR	NRR	NRR		NRR	NRR	NRR	NRR		NRR	NRR	NRR	NRR		NRR	NRR	NRR	NRR		NRR	NRR	NRR	NRR	
Transformers	PatchTST (2022)	1.002	1.007	1.028	1.044	0.020	1.008	1.011	1.011	0.985	0.011	1.005	1.026	1.055	1.050	0.032	1.00	1.004	1.017	1.035	0.014	1.004	1.022	1.082	1.134	<u>0.060</u>
	iTransformer (2023)	1.016	1.016	1.030	1.100	0.040	0.989	0.966	0.989	0.992	0.015	0.983	0.994	1.050	1.092	0.041	0.987	0.1020	1.074	1.098	0.051	1.010	1.112	1.456	1.692	0.318
	FrNet (2024)	0.994	0.997	1.021	1.035	<u>0.017</u>	1.006	1.003	1.024	1.033	0.016	1.017	1.023	1.032	1.056	0.032	1.000	1.004	1.050	1.091	0.036	1.000	1.069	1.191	1.240	0.125
CNN	ModernTCN (2024)	0.981	0.969	0.971	0.981	0.024	0.985	0.994	1.00	0.994	<u>0.008</u>	1.000	1.008	0.989	0.991	<u>0.006</u>	0.975	0.962	0.966	0.979	0.029	1.013	1.067	1.146	1.264	0.122
MLP	DLinear (2023)	0.983	0.973	0.976	0.985	0.020	0.0987	0.989	1.012	1.034	0.017	1.003	1.012	1.030	1.048	0.023	1.006	1.033	1.086	1.129	0.063	0.983	1.006	1.080	1.151	0.065
	SparseTSF (2024)	1.000	1.019	1.058	1.067	0.036	1.014	1.023	1.032	1.055	0.031	0.997	0.997	1.000	1.011	0.004	0.995	1.000	1.022	1.035	<u>0.015</u>	1.015	1.077	1.172	1.249	0.128
	FreTS (2024)	0.998	1.007	1.021	1.052	0.020	0.931	0.944	0.898	0.991	0.058	1.024	1.013	0.993	1.006	0.012	0.956	0.930	0.890	1.072	0.073	0.992	1.103	1.110	1.148	0.092
	HADL (w)	1.000	1.005	1.025	1.042	0.018	1.000	1.003	1.015	1.024	0.010	1.002	1.014	1.041	1.05	0.029	1.000	1.009	1.036	1.059	0.026	1.002	1.020	1.083	1.140	0.061
	HADL(w/o)	1.000	1.002	1.017	1.035	0.013	0.997	1.000	1.011	1.020	0.008	1.002	1.011	1.032	1.050	0.024	1.000	1.009	1.032	1.050	0.022	1.002	1.016	1.071	1.124	0.053

HADL achieves lowest MAV in ETTh1 (0.013), ETTh2 (0.008), and Traffic (0.053), indicating a strong resistance to noise. However, it underperforms on ETTm2 (0.022), where PatchTST (0.014) and SparseTSF (0.015) perform better.

The NRR score for HADL remains stable up to $\eta < 1.3$ (1.000 to 1.016), while other MLP models show greater variability starting from $\eta = 0.3$ (0.983 to 1.023) in ETT datasets. Compared to transformers, FrNet shows comparable NRR for $\eta < 1.3$ (0.994 to 1.023) in ETT datasets, and it degrades significantly in the Traffic dataset (1.000 to 1.069). PatchTST exhibits better noise resilience than other transformers across all datasets, but its NRR starts to fluctuate from $\eta \geq 0.7$ (≥ 1.007), whereas HADL remains more stable (≥ 1.000).

Combined Analysis HADL excels as a lightweight, noise-resilient forecasting model with strong overall accuracy. In ETTm2, it performs well in forecasting while remaining lightweight, but does not perform well in robustness, where PatchTST excels with a larger parameter count ($> 700K$). In contrast, on Traffic, HADL struggles in forecasting but achieves the highest robustness.

In particular, in ETTh1 and ETTh2, HADL ranks best in both multivariate forecasting and robustness, showcasing the effectiveness of its design. With strong MSE performance at minimal parameter cost and significantly lower FLOPs,

HADL emerges as a highly efficient alternative to heavier models like PatchTST, iTransformer, and FrNet while also proving to be a stronger contender against ultra-lightweight models such as SparseTSF.

6 Ablation Studies and Analysis

We conduct a series of experiments on ETTh1 and ETTh2 datasets to validate the effects of various components of the HADL framework. We use the rank = 40 for the low rank layer as part of the test, unless otherwise specified.

6.1 Effects of Haar Decomposition

We evaluate the significance of Haar decomposition by comparing the performance of our model with (w/) and without (w/o) this operation, as shown in Table 4.

The results indicate that models using Haar decomposition achieve similar or better accuracy compared to the without Haar setup while benefiting from reduced computational complexity and a 20–40% reduction in parameter size. This shows that Haar decomposition effectively compresses the input sequence by discarding noisy components, thereby maintaining or enhancing predictive performance.

Table 4: Comparison of MSE and count of total trainable parameters for ETTh1 and ETTh2 datasets for lookback window $L = 512$ and prediction length $H = \{96, 192, 336, 720\}$ for HADL framework with (w/) and without (w/o) Haar decomposition.

H		MSE		Parameters	
		w/ Haar	w/o Haar	w/ Haar	w/o Haar
ETTh1	96	0.362	0.362	14.18K	24.42K
	192	0.402	0.397	18.11K	26.35K
	336	0.421	0.421	24.02K	34.26K
	720	0.440	0.440	39.76K	50.0K
ETTh2	96	0.271	0.276	14.18K	24.42K
	192	0.333	0.335	18.11K	26.35K
	336	0.359	0.366	24.02K	34.26K
	720	0.394	0.396	39.76K	50.0K

We also examine the limitations of Haar decomposition with respect to the length of the lookback window (Appendix C.1). A short lookback window, after Haar decomposition, loses information due to halving the original length, which reduces the model’s accuracy. Thus, a sufficiently large or optimal lookback window is necessary for effective performance.

6.2 Effects of Low-Rank Layer

In this experiment, we evaluate the impact of replacing the low-rank layer with a standard linear layer. As shown in Table 5, the low-rank layer consistently outperforms the standard linear layer, achieving lower MSE while significantly reducing the parameter count, leading to enhanced computational efficiency. The improvement in MSE stems from the low-rank layer’s ability to focus on a smaller, more relevant subset of weights, thus minimizing the influence of noisy components in the time series.

Table 5: Comparison of MSE and count of parameters for ETTh1 and ETTh2 datasets for input sequence length $L = 512$ and prediction length $H = \{96, 192, 336, 720\}$ for HADL framework model with Low-Rank($r = 40$) and Standard Linear Layer. (*Bias is set to False.*)

H		MSE		Parameters	
		Low-Rank	Standard	Low-Rank	Standard
ETTh1	96	0.362	0.442	14.08K	24.58K
	192	0.397	0.463	17.92K	49.15K
	336	0.423	0.472	23.68K	86.02K
	720	0.420	0.487	39.04K	184.32K
ETTh2	96	0.274	0.312	14.08K	24.58K
	192	0.332	0.347	17.92K	49.15K
	336	0.364	0.361	24.02K	86.35K
	720	0.382	0.397	39.04K	184.32K

We also examine the weights of the low-rank versus standard linear matrices and observe that the standard linear layer has weights across a broad range of indices, while the low-rank layer has more focused and targeted weights (Appendix C.2).

The effectiveness of the low-rank layer is highly dependent on the choice of rank. The studies show that the optimal rank is crucial for achieving a balance between model simplicity and predictive performance (Appendix C.2).

6.3 Effects of Discrete Cosine Transform

In this experiment, we evaluate the impact of bypassing inversion from the frequency domain to the time domain during prediction, as discussed in Section 3.4. Figure 2 presents heat maps of low-rank matrix plots for $L = 512$ and $L = 96$ in the HADL framework with (w/) and without (w/o) DCT, using the ETTh1 dataset. The resulting MSE values are 0.362 (w/ DCT) and 0.371 (w/o DCT), indicating a slight improvement with DCT.

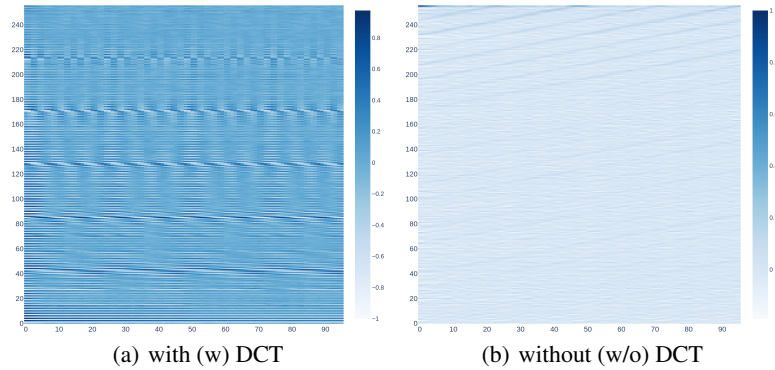


Figure 2: Heatmap plot of the Low-Rank Matrix for a lookback window $L = 512$ and a prediction length $H = 96$ in the HADL framework with (w/) and without (w/o) Discrete Cosine Transformation on the ETTh1 dataset.

The plots reveal that incorporating DCT enhances pattern clarity, distinguishing key structures more effectively than the model without DCT. While the DCT-enabled model tends to assign more positive weights, the non-DCT version exhibits more negative weights. Therefore, both approaches successfully identify and emphasize the critical components of the time series. This suggests that the low-rank layer can effectively learn essential features without requiring explicit inversion from the frequency domain to the time domain, as it inherently captures the extra weights typically introduced during inversion.

Further MSE evaluations across various prediction lengths show consistent improvements or comparable performance when using DCT, reinforcing its effectiveness in the HADL framework (Appendix C.3).

7 Discussion and Conclusion

In this work, we introduced HADL, a novel forecasting framework combining DWT and DCT for noise reduction and robust feature extraction, alongside a lightweight low-rank linear prediction layer, resulting in an efficient, noise-resilient, and accurate model for long-term multivariate time series forecasting.

However, there are several limitations that present opportunities for future improvement. One significant limitation of the HADL framework is its sensitivity to the size of the lookback window. While the model performs well with medium to large lookback windows, its accuracy degrades when the window is too small, primarily due to the reduced amount of historical information available for prediction. Conversely, when the lookback window is extended to ultra-long ranges, the model could potentially benefit from incorporating multiple levels of Haar decomposition. However, this introduces challenges, such as an increase in the number of trainable parameters. Additionally, the current strategy of discarding detail coefficients at each decomposition level must be revisited, as this may lead to the loss of important fine-grained information.

Despite these limitations, HADL outperforms ultra-lightweight models and remains highly efficient compared to transformer-based and MLP models, all while maintaining impressive robustness to noise and providing stable performance across varying noise levels. In conclusion, HADL framework offers a strong balance between forecasting

accuracy, parameter efficiency, and noise resilience, making it a highly competitive solution for long-term multivariate time series forecasting.

References

- [1] Sheikh Mohammad Idrees, M Afshar Alam, and Parul Agarwal. A prediction approach for stock market volatility based on time series data. *IEEE Access*, 7:17287–17298, 2019.
- [2] Jing Li, Muhammad Irfan, Sarminah Samad, Basit Ali, Yao Zhang, Daniel Badulescu, and Alina Badulescu. The relationship between energy consumption, co2 emissions, economic growth, and health indicators. *International Journal of Environmental Research and Public Health*, 20(3):2325, 2023.
- [3] Chirag Deb, Fan Zhang, Junjing Yang, Siew Eang Lee, and Kwok Wei Shah. A review on time series forecasting techniques for building energy consumption. *Renewable and Sustainable Energy Reviews*, 74:902–924, 2017.
- [4] Yusuf Yaslan and Bahadır Bican. Empirical mode decomposition based denoising method with support vector regression for time series prediction: A case study for electricity load forecasting. *Measurement*, 103:52–61, 2017.
- [5] Cameron Cornell, Nam Trong Dinh, and S Ali Pourmousavi. A probabilistic forecast methodology for volatile electricity prices in the australian national electricity market. *International Journal of Forecasting*, 2024.
- [6] Dattatray P Gandhmal and Kannan Kumar. Systematic analysis and review of stock market prediction techniques. *Computer Science Review*, 34:100190, 2019.
- [7] Ailing Zeng, Muxi Chen, Lei Zhang, and Qiang Xu. Are transformers effective for time series forecasting? In *Proceedings of the AAAI conference on artificial intelligence*, volume 37, pages 11121–11128, 2023.
- [8] Yuqi Nie, Nam H Nguyen, Phanwadee Sinthong, and Jayant Kalagnanam. A time series is worth 64 words: Long-term forecasting with transformers. *arXiv preprint arXiv:2211.14730*, 2022.
- [9] Yong Liu, Tengge Hu, Haoran Zhang, Haixu Wu, Shiyu Wang, Lintao Ma, and Mingsheng Long. itransformer: Inverted transformers are effective for time series forecasting. *arXiv preprint arXiv:2310.06625*, 2023.
- [10] Xinyu Zhang, Shanshan Feng, Jianghong Ma, Huiwei Lin, Xutao Li, Yunming Ye, Fan Li, and Yew Soon Ong. Frnet: Frequency-based rotation network for long-term time series forecasting. In *Proceedings of the 30th ACM SIGKDD Conference on Knowledge Discovery and Data Mining*, pages 3586–3597, 2024.
- [11] Zhijian Xu, Ailing Zeng, and Qiang Xu. Fits: Modeling time series with 10k parameters. *arXiv preprint arXiv:2307.03756*, 2023.
- [12] Shengsheng Lin, Weiwei Lin, Wentai Wu, Haojun Chen, and Junjie Yang. Sparsetsf: Modeling long-term time series forecasting with 1k parameters. *arXiv preprint arXiv:2405.00946*, 2024.
- [13] Vijay Ekambaram, Arindam Jati, Nam Nguyen, Phanwadee Sinthong, and Jayant Kalagnanam. Tsmixer: Lightweight mlp-mixer model for multivariate time series forecasting. In *Proceedings of the 29th ACM SIGKDD Conference on Knowledge Discovery and Data Mining*, pages 459–469, 2023.
- [14] Zhichen Lai, Dalin Zhang, Huan Li, Christian S Jensen, Hua Lu, and Yan Zhao. Lightcts: A lightweight framework for correlated time series forecasting. *Proceedings of the ACM on Management of Data*, 1(2):1–26, 2023.
- [15] Kun Yi, Qi Zhang, Wei Fan, Shoujin Wang, Pengyang Wang, Hui He, Ning An, Defu Lian, Longbing Cao, and Zhendong Niu. Frequency-domain mlps are more effective learners in time series forecasting. *Advances in Neural Information Processing Systems*, 36, 2024.
- [16] Donghao Luo and Xue Wang. Moderntcn: A modern pure convolution structure for general time series analysis. In *The Twelfth International Conference on Learning Representations*, 2024.
- [17] Shengsheng Lin, Weiwei Lin, Wentai Wu, Feiyu Zhao, Ruichao Mo, and Haotong Zhang. Segrnn: Segment recurrent neural network for long-term time series forecasting. *arXiv preprint arXiv:2308.11200*, 2023.
- [18] Musleh Alharthi and Ausif Mahmood. xlstmtime: Long-term time series forecasting with xlstm. *AI*, 5(3):1482–1495, 2024.
- [19] Yuxin Jia, Youfang Lin, Xinyan Hao, Yan Lin, Shengnan Guo, and Huaiyu Wan. Witran: Water-wave information transmission and recurrent acceleration network for long-range time series forecasting. *Advances in Neural Information Processing Systems*, 36, 2024.
- [20] Xinhe Liu and Wenmin Wang. Deep time series forecasting models: A comprehensive survey. *Mathematics*, 12(10):1504, 2024.
- [21] Xihao Piao, Zheng Chen, Taichi Murayama, Yasuko Matsubara, and Yasushi Sakurai. Fredformer: Frequency debiased transformer for time series forecasting. In *Proceedings of the 30th ACM SIGKDD Conference on Knowledge Discovery and Data Mining*, pages 2400–2410, 2024.

- [22] Edward J Hu, Yelong Shen, Phillip Wallis, Zeyuan Allen-Zhu, Yuanzhi Li, Shean Wang, Lu Wang, and Weizhu Chen. Lora: Low-rank adaptation of large language models. *arXiv preprint arXiv:2106.09685*, 2021.
- [23] Qingru Zhang, Minshuo Chen, Alexander Bukharin, Nikos Karampatziakis, Pengcheng He, Yu Cheng, Weizhu Chen, and Tuo Zhao. Adalora: Adaptive budget allocation for parameter-efficient fine-tuning. *arXiv preprint arXiv:2303.10512*, 2023.
- [24] Mojtaba Valipour, Mehdi Rezagholizadeh, Ivan Kobyzev, and Ali Ghodsi. Dylora: Parameter efficient tuning of pre-trained models using dynamic search-free low-rank adaptation. *arXiv preprint arXiv:2210.07558*, 2022.
- [25] Tong Nie, Yuewen Mei, Guoyang Qin, Jian Sun, and Wei Ma. Channel-aware low-rank adaptation in time series forecasting. In *Proceedings of the 33rd ACM International Conference on Information and Knowledge Management*, pages 3959–3963, 2024.
- [26] Nasir Ahmed, T_ Natarajan, and Kamisetty R Rao. Discrete cosine transform. *IEEE transactions on Computers*, 100(1):90–93, 1974.
- [27] Ingrid Daubechies and Bruce J Bates. Ten lectures on wavelets, 1993.
- [28] Yann Soon, Soo Ngee Koh, and Chai Kiat Yeo. Noisy speech enhancement using discrete cosine transform. *Speech communication*, 24(3):249–257, 1998.
- [29] Shahrzad Abbasi Baharanchi, Mansour Vali, and Mohammadreza Modaresi. Noise reduction of lung sounds based on singular spectrum analysis combined with discrete cosine transform. *Applied Acoustics*, 199:109005, 2022.
- [30] N Lee, T Ajanthan, and P Torr. Snip: single-shot network pruning based on connection sensitivity. In *International Conference on Learning Representations*. Open Review, 2019.
- [31] Steffen Schotthöfer, Emanuele Zangrando, Jonas Kusch, Gianluca Ceruti, and Francesco Tudisco. Low-rank lottery tickets: finding efficient low-rank neural networks via matrix differential equations. *Advances in Neural Information Processing Systems*, 35:20051–20063, 2022.
- [32] Sagar Imambi, Kolla Bhanu Prakash, and GR Kanagachidambaresan. Pytorch. *Programming with TensorFlow: solution for edge computing applications*, pages 87–104, 2021.
- [33] Pauli Virtanen, Ralf Gommers, Travis E. Oliphant, Matt Haberland, Tyler Reddy, David Cournapeau, Evgeni Burovski, Pearu Peterson, Warren Weckesser, Jonathan Bright, Stéfan J. van der Walt, Matthew Brett, Joshua Wilson, K. Jarrod Millman, Nikolay Mayorov, Andrew R. J. Nelson, Eric Jones, Robert Kern, Eric Larson, C J Carey, Ilhan Polat, Yu Feng, Eric W. Moore, Jake VanderPlas, Denis Laxalde, Josef Perktold, Robert Cimrman, Ian Henriksen, E. A. Quintero, Charles R. Harris, Anne M. Archibald, Antônio H. Ribeiro, Fabian Pedregosa, Paul van Mulbregt, and SciPy 1.0 Contributors. SciPy 1.0: Fundamental Algorithms for Scientific Computing in Python. *Nature Methods*, 17:261–272, 2020. doi: 10.1038/s41592-019-0686-2.
- [34] Haoyi Zhou, Shanghang Zhang, Jieqi Peng, Shuai Zhang, Jianxin Li, Hui Xiong, and Wancai Zhang. Informer: Beyond efficient transformer for long sequence time-series forecasting. In *Proceedings of the AAAI conference on artificial intelligence*, volume 35, pages 11106–11115, 2021.
- [35] Guokun Lai, Wei-Cheng Chang, Yiming Yang, and Hanxiao Liu. Modeling long-and short-term temporal patterns with deep neural networks. In *The 41st international ACM SIGIR conference on research & development in information retrieval*, pages 95–104, 2018.

Supplementary Material

A Benchmark Datasets

Table 6: Description of Benchmark Datasets

Dataset	ETTh1	ETTh2	ETTm1	ETTm2	Weather	Traffic	Electricity
Features	7	7	7	7	21	862	321
Timesteps	17420	17420	69680	69680	52697	17544	26304
Granularity	1 hour	1 hour	15 min	15 min	10 min	1 hour	15 min

Below is a description of benchmark datasets used:

- ETT¹ [34]: The Electricity Transformer Temperature captures station’s load and oil temperature recorded every 1 hour(ETTh1, ETTh2) and 15 mins(ETTm1, ETTm2) for two separate counties in China over a period of 2 years.
- Electricity² [35]: The Electricity Consumption Load is a collection of power consumption recorded in kWh for each household with 15 mins sampling rate. There are 321 household consumption recorded.
- Weather³ [34]: The climatological data consists of 21 meteorological features such as air temperature, humidity, etc. captured every 10 minutes for the year 2020.
- Traffic⁴ [35]: The data from California Department of Transportation describes road occupancy rates(between 0 and 1) measured by 862 different sensors on San Francisco Bay freeways hourly over a period of 48 months.

¹<https://github.com/zhouhaoyi/ETDataset>

²<https://github.com/laiquokun/multivariate-time-series-data>

³<https://www.bgc-jena.mpg.de/wetter/>

⁴<https://github.com/laiquokun/multivariate-time-series-data>

B Alogrithm

The algorithm formally summarizes the necessary steps for the HADL framework.

Algorithm 1 HADL Time Series Forecasting

1: **Input:** Multivariate time series $X_T \in \mathbb{R}^{C \times L}$, lookback window L , horizon length H

2: **Output:** Predicted values $\hat{Y}_T \in \mathbb{R}^{C \times H}$

3: **Step 1: Wavelet Decomposition**

4: Apply Discrete Wavelet Transform (DWT) with Haar Wavelet:

$$A_{T,-} \leftarrow \text{DWT}(X_T)$$

5: Retain approximation coefficients $A_T \in \mathbb{R}^{C \times \frac{L}{2}}$ to reduce noise.

6: **Step 2: Frequency Domain Transformation**

7: Transform approximation coefficients into the frequency domain using Discrete Cosine Transform (DCT):

$$A_F \leftarrow \text{DCT}(A_T)$$

8: Normalize the frequency representation:

$$A_F \leftarrow \frac{2}{L} \cdot A_F$$

9: **Step 3: Low-Rank Prediction**

10: Map the frequency representation $A_F \in \mathbb{R}^{C \times \frac{L}{2}}$ to the target forecast in the time domain using a low-rank layer:

$$\hat{Y}_T \leftarrow \text{LowRankLayer}(A_F)$$

11: **Return:** Predicted values \hat{Y}_T

C Additional Ablation Studies

C.1 Haar decomposition Testing

Table 7 presents the results of the HADL framework for lookback windows $L = \{48, 96, 192, 336, 512, 720\}$ and prediction lengths $H = \{96, 192, 336, 720\}$ on the ETTh1 and ETTh2 datasets with rank $r = 40$. The results highlight a limitation of the HADL for smaller lookback windows, where accuracy deteriorates. This is likely due to the halving of the original time series length, which may result in the loss of critical information necessary for accurate predictions when the lookback window is too small.

Table 7: Results of the HADL framework in MSE for lookback windows $L = \{48, 96, 192, 336, 512, 720\}$ and prediction lengths $H = \{96, 192, 336, 720\}$

		H				
		L	96	192	336	720
ETTh1	48	0.400	0.452	0.502	0.501	
	96	0.385	0.435	0.476	0.470	
	192	0.377	0.422	0.451	0.443	
	336	0.368	0.403	0.427	0.432	
	512	0.362	0.402	0.421	0.440	
	720	0.371	0.405	0.442	0.454	
ETTh2	48	0.302	0.394	0.445	0.450	
	96	0.290	0.375	0.414	0.421	
	192	0.284	0.356	0.385	0.409	
	336	0.275	0.336	0.361	0.397	
	512	0.271	0.333	0.359	0.394	
	720	0.274	0.335	0.360	0.398	

Table 8 presents the results for varying ranks $r = \{15, 35, 55, 75\}$ in the low-rank layer, with a window size of $L = 512$ and prediction lengths $H = \{96, 192, 336, 720\}$ for the ETTh1 and ETTh2 datasets. The results suggest that a very low rank reduces accuracy due to a reduced number of parameters. An optimal rank strikes a balance, providing good accuracy without excessive memory requirements.

Table 8: Results of the HADL framework in MSE for a lookback window of $L = 512$, prediction lengths $H = \{96, 192, 336, 720\}$ and Low Rank Layer with rank $r = \{15, 35, 55, 75\}$ for ETTh1 and ETTh2 datasets.

		MSE				Parameters			
		H	r	15	35	55	75	15	35
ETTh1	96	0.367	0.369	0.362	0.363	5.38K	12.42K	19.46K	26.5K
	192	0.401	0.404	0.395	0.395	6.91K	15.87K	24.83K	33.79K
	336	0.426	0.422	0.421	0.421	9.22K	21.06K	32.9K	44.74K
	720	0.445	0.445	0.442	0.435	15.36K	34.88K	54.4K	73.92K
ETTh2	96	0.274	0.270	0.270	0.271	5.38K	12.42K	19.46K	26.5K
	192	0.335	0.334	0.333	0.331	6.91K	15.87K	24.83K	33.79K
	336	0.364	0.359	0.358	0.357	9.22K	21.06K	32.9K	44.74K
	720	0.398	0.396	0.393	0.392	15.36K	34.88K	54.4K	73.92K

C.2 Low Rank Testing

Figure 3 presents a heatmap comparing low-rank and standard linear matrices for $L = 512$ and $H = 96$ in the HADL framework, without bias, for the ETTh1 dataset. The results indicate that the low-rank approach assigns weights less aggressively compared to the standard linear layer, thereby reducing the influence of noisy components that are weighted more heavily in the standard linear layer.

Figure 3 and Table 5 demonstrate that the generalization capability of the low-rank approach helps mitigate noise in time series data. Moreover, it achieves comparable outputs with fewer parameters and lower memory requirements.

C.3 Discrete Cosine Transform Testing

We investigate the impact of incorporating the DCT in our model by removing the DCT operation and evaluating the model’s MSE based on predictions directly from the time domain. Without the DCT, the low-rank layer relies solely on the input transformed by the Haar decomposition, which operates in the time domain instead of the frequency domain.

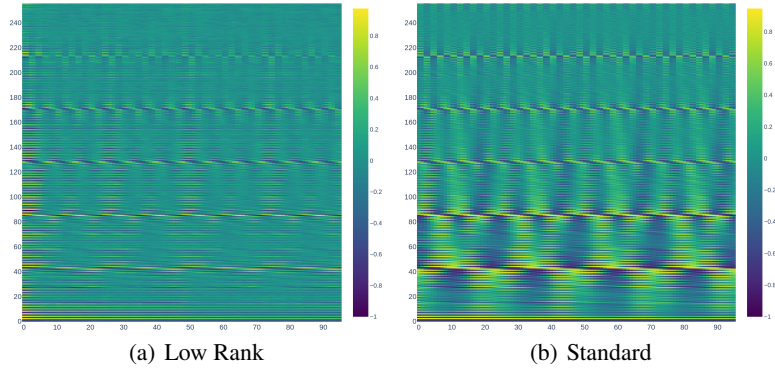


Figure 3: Heatmap plot for HADL framework comparing the Standard Linear and Low-Rank Matrices for a lookback window $L = 512$ and a prediction length $H = 96$ for ETTh1 dataset. Bias is set to *False*.

Table 9: MSE results for the HADL framework with (w/) and without (w/o) Discrete Cosine Transformation, for a lookback window $L = 512$ and prediction lengths $H = \{96, 192, 336, 720\}$ on the ETTh1 and ETTh2 datasets.

		MSE	
		w/ DCT	w/o DCT
ETTh1	H		
	96	0.362	0.371
	192	0.402	0.402
	336	0.421	0.432
ETTh2	720	0.440	0.438
	96	0.271	0.277
	192	0.333	0.337
	336	0.359	0.359
	720	0.394	0.396

The results in Table 9 indicate that the model with DCT either outperforms or achieves similar MSE values compared to the model without DCT across both datasets.

D Results

D.1 Multivariate Forecasting

Table 10 presents the results of multivariate long-term time series forecasting, evaluated using MSE and MAE, across all benchmark datasets. It compares the performance of SOTA models with a lookback window of $L = 512$ and prediction lengths $H = \{96, 192, 336, 720\}$ to that of the HADL framework, both with (w/) and without (w/o) L1 regularization. All models were trained for 100 epochs with a patience level of 20.

Table 10: Results in MSE and MAE (lower is better) for multivariate long-term time series forecasting on benchmark datasets. We compare against baseline models using a standard prediction length $H = \{96, 192, 336, 720\}$ and a lookback window $L = 512$ for all models.

Dataset	H	MLP										Transformers				CNN			
		HADL (w/)		HADL (w/o)		DLinear (2023)		SparseTSF (2024)		FreTS (2024)		PatchTST (2022)		iTransformer (2023)		FrNet (2024)		ModemTCN (2024)	
		MSE	MAE	MSE	MAE	MSE	MAE	MSE	MAE	MSE	MAE	MSE	MAE	MSE	MAE	MSE	MAE	MSE	MAE
ETTh1	96	0.363	0.393	0.365	0.394	0.382	0.403	0.392	0.408	0.396	0.420	0.394	0.419	0.399	0.423	0.362	0.392	0.385	0.411
	192	0.395	0.414	0.397	0.414	0.418	0.426	0.412	0.421	0.435	0.448	0.424	0.440	0.428	0.444	0.390	0.415	0.421	0.430
	336	0.421	0.429	0.423	0.429	0.455	0.469	0.425	0.432	0.471	0.472	0.457	0.467	0.472	0.474	0.427	0.436	0.448	0.448
	720	0.444	0.462	0.446	0.462	0.496	0.498	0.425	0.453	0.565	0.551	0.461	0.475	0.531	0.520	0.468	0.478	0.531	0.511
ETTh2	96	0.271	0.336	0.272	0.335	0.354	0.391	0.285	0.345	0.318	0.383	0.292	0.355	0.301	0.359	0.269	0.336	0.300	0.356
	192	0.334	0.378	0.334	0.377	0.512	0.481	0.345	0.382	0.432	0.453	0.347	0.396	0.381	0.408	0.330	0.378	0.348	0.389
	336	0.358	0.403	0.358	0.402	0.603	0.536	0.364	0.400	0.479	0.483	0.380	0.423	0.395	0.427	0.358	0.405	0.384	0.420
	720	0.395	0.440	0.395	0.439	1.060	0.722	0.384	0.424	0.809	0.650	0.431	0.453	0.460	0.468	0.391	0.432	0.410	0.440
ETTm1	96	0.304	0.349	0.306	0.349	0.292	0.338	0.330	0.365	0.317	0.360	0.293	0.344	0.315	0.367	0.295	0.347	0.310	0.361
	192	0.337	0.367	0.339	0.368	0.333	0.362	0.347	0.372	0.356	0.384	0.335	0.367	0.350	0.389	0.337	0.371	0.354	0.387
	336	0.365	0.383	0.367	0.383	0.368	0.382	0.374	0.388	0.385	0.404	0.368	0.387	394	0.416	0.363	0.380	0.392	0.402
	720	0.418	0.414	0.420	0.413	0.428	0.417	0.424	0.415	0.440	0.434	0.423	0.420	0.446	0.445	0.421	0.415	0.446	0.435
ETTm2	96	0.163	0.253	0.163	0.252	0.204	0.288	0.173	0.260	0.179	0.263	0.164	0.254	0.188	0.275	0.165	0.254	0.169	0.261
	192	0.218	0.290	0.218	0.290	0.333	0.362	0.225	0.294	0.254	0.313	0.223	0.294	0.250	0.317	0.221	0.293	0.232	0.303
	336	0.271	0.325	0.271	0.325	0.342	0.386	0.277	0.328	0.314	0.354	0.277	0.329	0.326	0.361	0.274	0.328	0.307	0.349
	720	0.359	0.382	0.359	0.382	0.570	0.488	0.362	0.382	0.389	0.412	0.381	0.395	0.391	0.408	0.360	0.387	0.385	0.399
Traffic	96	0.413	0.299	0.413	0.294	0.418	0.298	0.413	0.299	0.398	0.278	0.489	0.354	0.433	0.324	0.367	0.274	0.392	0.285
	192	0.433	0.312	0.433	0.308	0.430	0.303	0.433	0.312	0.414	0.285	0.498	0.357	0.462	0.343	0.390	0.286	0.406	0.291
	336	0.445	0.317	0.444	0.314	0.440	0.309	0.445	0.317	0.428	0.291	0.506	0.360	0.443	0.323	0.397	0.283	0.415	0.296
	720	0.481	0.335	0.481	0.332	0.479	0.331	0.481	0.335	0.471	0.313	0.541	0.376	0.489	0.349	0.433	0.301	0.464	0.327
Weather	96	0.171	0.224	0.170	0.223	0.142	0.204	0.179	0.233	0.181	0.252	0.145	0.198	0.158	0.210	0.143	0.196	0.156	0.212
	192	0.215	0.261	0.214	0.260	0.186	0.251	0.220	0.265	0.222	0.290	0.189	0.239	0.203	0.249	0.185	0.236	0.202	0.253
	336	0.260	0.295	0.260	0.295	0.236	0.294	0.264	0.298	0.278	0.330	0.239	0.278	0.263	0.295	0.234	0.274	0.255	0.294
	720	0.326	0.343	0.326	0.342	0.311	0.354	0.328	0.343	0.346	0.386	0.311	0.331	0.329	0.344	0.309	0.330	0.347	0.354
Electricity	96	0.151	0.256	0.149	0.252	0.132	0.229	0.151	0.248	0.191	0.310	0.157	0.265	0.148	0.250	0.132	0.227	0.139	0.242
	192	0.168	0.271	0.166	0.267	0.148	0.245	0.164	0.259	0.215	0.331	0.172	0.277	0.168	0.270	0.147	0.239	0.154	0.253
	336	0.183	0.286	0.181	0.282	0.164	0.263	0.180	0.278	0.258	0.368	0.188	0.291	0.175	0.274	0.163	0.257	0.172	0.275
	720	0.222	0.317	0.220	0.313	0.201	0.297	0.218	0.308	0.276	0.378	0.224	0.320	0.216	0.309	0.200	0.290	0.209	0.301

D.2 Univariate Long-Term Forecasting

Table 11 presents the results of univariate long-term time series forecasting, evaluated using MSE and MAE, across all benchmark datasets. The table compares SOTA models with a lookback window of $L = 512$ and prediction lengths of $H = \{96, 192, 336, 720\}$ to the performance of the HADL framework, both with (w/) and without (w/o) L1 regularization. All models are trained for 50 epochs with a patience level of 10.

Table 11: Results in MSE and MAE (lower is better) for univariate long-term time series forecasting on benchmark datasets. We compare with baseline models with standard prediction length $H = \{96, 192, 336, 720\}$ and input sequence $L = 512$ for all models.

Dataset	H	MLP										Transformers				CNN			
		HADL (w/)		HADL (w/o)		DLinear (2023)		SparseTSF (2024)		FreTS (2024)		PatchTST (2022)		iTransformer (2023)		FrNet (2024)		ModemTCN (2024)	
		MSE	MAE	MSE	MAE	MSE	MAE	MSE	MAE	MSE	MAE	MSE	MAE	MSE	MAE	MSE	MAE	MSE	MAE
ETTh1	96	0.101	0.244	0.100	0.244	0.064	0.191	0.064	0.199	0.095	0.241	0.069	0.205	0.085	0.230	0.054	0.180	0.080	0.223
	192	0.116	0.264	0.116	0.264	0.085	0.223	0.080	0.223	0.114	0.266	0.083	0.227	0.091	0.239	0.067	0.204	0.085	0.236
	336	0.129	0.282	0.127	0.280	0.108	0.257	0.090	0.240	0.122	0.277	0.091	0.242	0.099	0.249	0.080	0.225	0.088	0.236
	720	0.167	0.322	0.169	0.324	0.191	0.361	0.107	0.256	1.794	0.333	0.106	0.256	0.131	0.289	0.095	0.240	0.108	0.262
ETTh2	96	0.189	0.346	0.202	0.361	0.139	0.290	0.152	0.309	0.179	0.333	0.160	0.318	0.278	0.430	0.132	0.283	0.245	0.404
	192	0.225	0.383	0.235	0.392	0.181	0.336	0.187	0.347	0.227	0.384	0.192	0.352	0.296	0.445	0.168	0.324	0.258	0.416
	336	0.255	0.411	0.263	0.420	0.204	0.364	0.204	0.366	0.316	0.440	0.209	0.372	0.312	0.456	0.178	0.343	0.270	0.426
	720	0.339	0.474	0.364	0.493	0.334	0.470	0.241	0.394	0.325	0.464	0.252	0.406	0.405	0.519	0.221	0.376	0.347	0.481
ETTm1	96	0.026	0.123	0.026	0.122	0.026	0.122	0.028	0.130	1.679	0.703	0.027	0.126	0.051	0.176	0.026	0.122	0.0384	0.152
	192	0.039	0.150	0.039	0.150	0.041	0.151	0.041	0.155	4.594	1.156	0.040	0.153	0.061	0.191	0.040	0.152	0.049	0.171
	336	0.052	0.173	0.051	0.173	0.055	0.175	0.053	0.176	2.945	0.879	0.053	0.175	0.067	0.199	0.053	0.175	0.060	0.188
	720	0.070	0.203	0.070	0.204	0.075	0.205	0.072	0.206	8.60	1.518	0.072	0.205	0.085	0.226	0.072	0.206	0.077	0.215
ETTm2	96	0.063	0.185	0.063	0.185	0.063	0.183	0.071	0.202	0.140	0.264	0.069	0.199	0.077	0.213	0.065	0.188	0.097	0.243
	192	0.090	0.226	0.90	0.226	0.091	0.226	0.096	0.238	0.565	0.418	0.095	0.235	0.105	0.253	0.094	0.232	0.118	0.267
	336	0.118	0.261	0.118	0.261	0.120	0.263	0.122	0.269	1.615	0.601	0.121	0.267	0.134	0.287	0.124	0.271	0.140	0.292
	720	0.171	0.321	0.171	0.321	0.174	0.321	0.175	0.325	5.742	1.048	0.173	0.323	0.186	0.344	0.178	0.329	0.190	0.342
Electricity	96	0.227	0.342	0.245	0.358	0.192	0.303	0.234	0.343	0.287	0.398	0.258	0.384	0.237	0.345	0.210	0.314	0.196	0.307
	192	0.263	0.367	0.283	0.385	0.225	0.326	0.262	0.362	0.331	0.425	0.287	0.384	0.276	0.374	0.244	0.341	0.231	0.331
	336	0.297	0.393	0.314	0.408	0.260	0.355	0.289	0.383	0.393	0.468	0.314	0.404	0.283	0.382	0.285	0.372	0.270	0.361
	720	0.344	0.440	0.364	0.456	0.294	0.397	0.339	0.433	0.722	0.549	0.358	0.449	0.331	0.427	0.351	0.442	0.317	0.411
Weather	96	0.001	0.030	0.001	0.024	0.005	0.058	0.001	0.024	0.005	0.061	0.001	0.027	0.001	0.275	0.001	0.025	0.001	0.025
	192	0.001	0.031	0.001	0.0026	0.005	0.062	0.001	0.027	0.006	0.064	0.001	0.028	0.001	0.029	0.001	0.027	0.001	0.028
	336	0.001	0.032	0.001	0.028	0.006	0.065	0.001	0.028	0.006	0.065	0.001	0.030	0.001	0.030	0.001	0.029	0.001	0.030
	720	0.002	0.036	0.002	0.033	0.006	0.069	0.002	0.033	0.006	0.068	0.002	0.035	0.002	0.035	0.002	0.034	0.002	0.035
Traffic	96	0.308	0.417	0.304	0.408	0.118	0.197	0.276	0.377	3.184	1.017	0.297	0.396	0.251	0.356	0.138	0.231	0.707	0.649
	192	0.315	0.422	0.311	0.412	0.120	0.199	0.275	0.375	3.27	1.13	0.297	0.396	0.275	0.375	0.134	0.223	0.717	0.654
	336	0.316	0.424	0.311	0.415	0.119	0.202	0.264	0.366	5.805	1.445	0.295	0.4396	0.260	0.364	0.142	0.243	0.756	0.670
	720	0.332	0.437	0.327	0.428	0.135	0.224	0.305	0.400	3.02	1.100	0.315	0.410	0.289	0.387	0.153	0.251	0.799	0.688

D.3 Robustness Testing

Table 12 presents a comparison of the HADL framework with baseline models, reported in terms of MSE and MAE across all benchmark datasets. Robustness testing was conducted by introducing noise into the training data ($X_{\text{train}}, y_{\text{train}}$) using the formula:

$$X_{\text{train}} := X_{\text{train}} + \mathcal{N}(0, 1) * \eta \quad (12)$$

Here $\mathcal{N}(0, 1)$ represents random noise sampled from a standard normal distribution, and $\eta = \{0.0, 0.3, 0.7, 1.7, 2.3\}$ controls the noise intensity. The validation and test datasets remained unchanged to ensure a consistent and unbiased evaluation of model robustness. All models are trained for 50 epochs with a patience level of 10.

Table 12: MSE and MAE results for robustness testing on benchmark datasets, comparing our HADL framework with (w/) and without (w/o) regularization against baseline models. The tests are conducted using a lookback window of $L = 512$ and a prediction length of $H = 192$ under varying noise intensities $\eta = \{0.0, 0.3, 0.7, 1.3, 1.7, 2.3\}$.

Dataset	H	MLP										Transformers				CNN			
		HADL (w/)		HADL (w/o)		DLinear (2023)		SparseTSF (2024)		FreTS (2024)		PatchTST (2022)		iTransformer (2023)		FrNet (2024)		ModernTCN (2024)	
		MSE	MAE	MSE	MAE	MSE	MAE	MSE	MAE	MSE	MAE	MSE	MAE	MSE	MAE	MSE	MAE	MSE	MAE
ETTh1	0.0	0.396	0.414	0.397	0.414	0.422	0.429	0.412	0.421	0.517	0.503	0.427	0.442	0.427	0.443	0.396	0.416	0.421	0.430
	0.3	0.396	0.414	0.397	0.414	0.415	0.424	0.412	0.422	0.516	0.504	0.428	0.443	0.434	0.448	0.394	0.414	0.413	0.425
	0.7	0.398	0.417	0.398	0.417	0.411	0.423	0.420	0.430	0.521	0.506	0.430	0.445	0.434	0.447	0.395	0.415	0.408	0.426
	1.3	0.406	0.424	0.404	0.423	0.412	0.428	0.436	0.441	0.528	0.510	0.439	0.453	0.440	0.449	0.406	0.425	0.409	0.426
	1.7	0.413	0.429	0.411	0.427	0.416	0.433	0.440	0.443	0.544	0.519	0.446	0.458	0.470	0.463	0.410	0.427	0.413	0.429
2.3	0.427	0.437	0.423	0.435	0.424	0.441	0.454	0.451	0.575	0.536	0.459	0.466	0.525	0.490	0.423	0.435	0.422	0.435	
ETTh2	0.0	0.333	0.377	0.334	0.377	0.547	0.490	0.343	0.381	0.581	0.534	0.348	0.396	0.383	0.409	0.329	0.379	0.337	0.387
	0.3	0.333	0.377	0.333	0.377	0.540	0.483	0.348	0.382	0.541	0.510	0.351	0.398	0.379	0.404	0.331	0.377	0.332	0.381
	0.7	0.334	0.379	0.334	0.378	0.541	0.485	0.351	0.385	0.549	0.517	0.352	0.398	0.370	0.400	0.330	0.376	0.335	0.380
	1.3	0.338	0.382	0.338	0.381	0.554	0.494	0.354	0.390	0.522	0.505	0.352	0.398	0.379	0.403	0.337	0.379	0.340	0.382
	1.7	0.341	0.385	0.341	0.384	0.566	0.501	0.362	0.396	0.576	0.531	0.343	0.390	0.380	0.406	0.340	0.382	0.335	0.380
2.3	0.346	0.390	0.345	0.388	0.587	0.513	0.368	0.401	0.524	0.510	0.343	0.391	0.386	0.414	0.345	0.386	0.346	0.387	
ETTm1	0.0	0.336	0.366	0.338	0.367	0.333	0.362	0.355	0.377	0.446	0.459	0.335	0.367	0.356	0.394	0.336	0.368	0.369	0.396
	0.3	0.337	0.367	0.339	0.367	0.334	0.362	0.354	0.377	0.457	0.468	0.337	0.368	0.350	0.390	0.342	0.373	0.369	0.393
	0.7	0.341	0.372	0.342	0.371	0.337	0.366	0.354	0.378	0.452	0.461	0.344	0.374	0.354	0.391	0.344	0.375	0.372	0.395
	1.3	0.350	0.380	0.349	0.379	0.343	0.374	0.355	0.383	0.443	0.453	0.350	0.380	0.374	0.405	0.347	0.379	0.365	0.392
	1.7	0.356	0.386	0.355	0.384	0.349	0.380	0.359	0.387	0.449	0.457	0.352	0.382	0.389	0.414	0.355	0.385	0.366	0.394
2.3	0.369	0.395	0.366	0.393	0.358	0.389	0.371	0.396	0.452	0.459	0.360	0.390	0.408	0.422	0.359	0.394	0.370	0.400	
ETTm2	0.0	0.218	0.290	0.218	0.290	0.302	0.355	0.225	0.296	0.347	0.406	0.223	0.295	0.243	0.312	0.219	0.292	0.241	0.313
	0.3	0.218	0.290	0.218	0.290	0.304	0.356	0.224	0.295	0.332	0.398	0.223	0.295	0.240	0.309	0.219	0.292	0.235	0.307
	0.7	0.220	0.293	0.220	0.292	0.312	0.363	0.225	0.296	0.323	0.390	0.224	0.297	0.248	0.314	0.220	0.293	0.232	0.303
	1.3	0.226	0.298	0.225	0.297	0.328	0.376	0.230	0.300	0.309	0.382	0.227	0.297	0.261	0.323	0.230	0.302	0.233	0.304
	1.7	0.231	0.303	0.229	0.301	0.341	0.386	0.233	0.304	0.372	0.419	0.231	0.302	0.267	0.329	0.239	0.309	0.236	0.307
2.3	0.238	0.309	0.236	0.308	0.363	0.402	0.239	0.310	0.335	0.401	0.234	0.304	0.266	0.334	0.239	0.309	0.243	0.313	
Traffic	0.0	0.433	0.311	0.433	0.308	0.430	0.303	0.441	0.309	0.417	0.286	0.498	0.357	0.462	0.343	0.387	0.283	0.431	0.304
	0.3	0.434	0.311	0.434	0.308	0.423	0.299	0.448	0.329	0.414	0.287	0.500	0.357	0.467	0.345	0.387	0.283	0.437	0.309
	0.7	0.442	0.315	0.440	0.310	0.433	0.305	0.475	0.325	0.460	0.298	0.509	0.361	0.514	0.382	0.414	0.317	0.460	0.324
	1.3	0.469	0.332	0.464	0.325	0.468	0.324	0.517	0.354	0.463	0.317	0.539	0.376	0.673	0.482	0.461	0.361	0.494	0.382
	1.7	0.494	0.347	0.487	0.338	0.495	0.338	0.551	0.376	0.479	0.326	0.565	0.389	0.782	0.537	0.480	0.374	0.545	0.374
2.3	0.534	0.370	0.525	0.361	0.537	0.359	0.623	0.432	0.505	0.338	0.601	0.407	0.716	0.518	0.482	0.380	0.596	0.403	
Weather	0.0	0.214	0.260	0.214	0.260	0.184	0.249	0.222	0.268	0.222	0.290	0.189	0.239	0.202	0.249	0.186	0.236	0.196	0.246
	0.3	0.215	0.262	0.214	0.260	0.189	0.255	0.222	0.268	0.225	0.294	0.191	0.243	0.208	0.253	0.200	0.246	0.206	0.251
	0.7	0.217	0.265	0.216	0.263	0.195	0.262	0.222	0.268	0.235	0.305	0.197	0.249	0.219	0.264	0.224	0.268	0.212	0.256
	1.3	0.222	0.270	0.221	0.269	0.202	0.271	0.225	0.272	0.230	0.293	0.204	0.256	0.227	0.275	0.226	0.273	0.215	0.261
	1.7	0.225	0.274	0.224	0.273	0.207	0.277	0.228	0.275	0.229	0.291	0.208	0.259	0.234	0.280	0.227	0.275	0.213	0.262
2.3	0.230	0.280	0.229	0.278	0.214	0.287	0.231	0.280	0.230	0.290	0.215	0.266	0.243	0.288	0.231	0.279	0.218	0.269	
Electricity	0.0	0.168	0.271	0.168	0.271	0.148	0.245	0.164	0.259	0.215	0.331	0.172	0.277	0.168	0.270	0.146	0.239	0.175	0.279
	0.3	0.169	0.272	0.168	0.272	0.148	0.246	0.168	0.266	0.219	0.334	0.174	0.279	0.174	0.277	0.156	0.254	0.174	0.279
	0.7	0.175	0.279	0.174	0.277	0.154	0.256	0.188	0.288	0.219	0.334	0.180	0.286	0.206	0.318	0.167	0.269	0.178	0.285
	1.3	0.189	0.294	0.189	0.293	0.167	0.274	0.212	0.311	0.233	0.346	0.193	0.301	0.313	0.426	0.191	0.298	0.184	0.293
	1.7	0.200	0.305	0.199	0.304	0.176	0.285	0.229	0.328	0.245	0.355	0.202	0.310	0.351	0.456	0.207	0.317	0.188	0.297
2.3	0.217	0.321	0.216	0.320	0.190	0.301	0.258	0.345	0.253	0.362	0.218	0.327	0.424	0.510	0.233	0.344	0.194	0.303	